Journal of Metals, Materials and Minerals, 35(1), e2105, 2025

Investigation of photocathodic corrosion protection of ZnO/ZnS thin film for AISI 304 stainless steel in 3.5 wt% NaCl solution

Soravid VEERAPONG[1], Naw Blessing OO[1], Boossayamas DACHBUMROONG[2], Parichart CHAUM[2], Thanate NA WICHEAN[2], Oratai JONGPRATEEP[1,3], Naray PEWNIM[1,3], Gasidit PANOMSUWAN[1,3], and Ratchatee TECHAPIESANCHAROENKIJ[1,3,*]

[1] *Department of Materials Engineering, Faculty of Engineering, Kasetsart University, 50 Ngam Wong Wan Rd., Ladyao, Chatuchak, Bangkok, 10900, Thailand*

[2] *Materials Innovation Center, Faculty of Engineering, Kasetsart University, 50 Ngam Wong Wan Rd., Ladyao, Chatuchak, Bangkok, 10900, Thailand*

[3] *Special Research Unit for Biomass Conversion Technology for Energy and Environment, Department of Materials Engineering, Faculty of Engineering, Kasetsart University, 50 Ngam Wong Wan Rd, Ladyao Chatuchak Bangkok, 10900, Thailand*

***Corresponding author e-mail**: fengrct@ku.ac.th

Received date:
16 July 2024
Revised date:
20 November 2024
Accepted date:
4 January 2025

Keywords:
ZnO;
ZnS;
Heterostructure semiconductors;
Photoelectrochemistry;
Corrosion

Abstract

Photocathodic protection is an alternative cathodic protection technique to protect metals by photo-generated electrons from a coupled semiconductor film under solar light. In this report, ZnO nanorods and heterostructure ZnO/ZnS nanorod films on FTO substrates were studied for their photocathodic protection for 304 stainless steels (304 SS) in a 3.5 wt% NaCl solution. The ZnO and ZnO/ZnS nanorods were fabricated on FTO substrates by spray pyrolysis and hydrothermal processes. The photocathodic performances of the ZnO and ZnO/ZnS photoanodes coupled with 304 SS samples were examined by Open-Circuit Potential (OCP), polarization curve analysis, and electrochemical impedance spectra (EIS). The ZnO/ZnS photoanodes showed better photocathodic performance than the ZnO photoanodes with larger negative potential shifts and higher photo-generated current density under light illumination. The ZnO/ZnS heterostructure films show promising photocathodic protection for 304 SS under chloride atmosphere. However, both ZnO and ZnO/ZnS failed to provide any protection under dark conditions.

1. Introduction

In the present day, metals are extensively used in areas around oceans where metals can rapidly corrode due to high temperatures, humidity, and elevated salt content in the environment [1-3]. The use of metals in seawater poses continuous challenges and potential property loss due to corrosion, necessitating constant maintenance and repair. Seawater typically contains around 3.5 wt% NaCl, constituting the highest concentration of NaCl affecting metals [4]. Therefore, a 3.5 wt% NaCl solution is recommended in most research and international standards, i.e. ASTM, for corrosion and coating studies to simulate an environment similar to marine environments [4-6].

To mitigate the loss caused by corrosion in seawater, various techniques are available. Methods such as applying coatings can partially prevent corrosion, albeit at the expense of the time required for reapplication. Electrochemical protections, including impressed current cathodic protection (ICCP) and sacrificial anode cathodic protection (SACP), are fully favored for their effectiveness in safeguarding metallic structures in marine environments or on vessels at sea [7]. Photocathodic protection (PCP) is a promising technique in preventing metal corrosion. It not only provides alternative electrical energy similar to ICCP but also harnesses clean energy from sunlight. During PCP process [8], a metal can be cathodically protected by a photoanode under sunlight irradiation. When exposed to sunlight, electrons are generated from the n-type semiconductor material and transported to the connected metal, thereby reducing its susceptibility to corrosion.

In general, n-type semiconductor materials such as TiO_2 and ZnO are commonly preferred due to their excellent photoelectrochemical performance (PCP) [9-14]. Numerous studies have been conducted on these materials as they possess conduction band levels higher than the corrosion potential of materials like SS304 and carbon steel. However, the efficiency of the PCP process using TiO_2 and ZnO is still limited, primarily due to their low light absorption capacity [9,12]. Heterostructure semiconductor films of multiple n-type semiconductor materials with varying band gap energies may be applied to enhance sunlight absorption [8-10,13]. ZnS has conduction band (CB) and valence band (VB) levels higher than those of ZnO. The composite films of ZnS and ZnO can enhance the efficiency of the photo-electrochemical protection (PCP) process. The heterojunction between ZnO and ZnS promotes a photocurrent and open-circuit potential (OCP) shift, due to the electron-hole separation at the junction [14-15]. All prior studies reported the performance of the photoanode cells

in hole-scavenger solutions, e.g. Na_2S-NaOH. There has not been reports of the performances of both working electrodes and coupled photoanodes in a 3.5 wt% NaCl solution of a simulated marine condition.

Extensive studies on ZnO coating on a 304 stainless steel metal substrate by a spray pyrolysis technique, aiming to explore PCP performance, have been widely reported [16-20]. This approach proves effective in preventing corrosion and convenient for synthesis, providing a uniform surface of ZnO on a SS304 substrate. A drawback of the ZnO spray pyrolysis synthesis is the use of high temperatures (above 200°C), causing changes in the surface properties of the SS304 metal [16]. Subsequent studies have attempted ZnO synthesis using the spray pyrolysis on 304 SS metal at lower temperatures, and the results indicate that corrosion can be prevented using the PCP method during testing. Nevertheless, the 304 SS metal still underwent corrosion during the spray pyrolysis process, leading to changes in the metal surface [17]. Nevertheless, the spray pyrolysis technique is easy and cheap to perform and allows for controlled deposition with a clear structure, which is ideal for scaling up processes. Therefore, to avoid oxidation on a metal substrate, an application of the spray pyrolysis technique to fabricate semiconductor oxide films on an inert glass substrate is an alternative process for preparing a separated photoanode, which can be electrically coupled with a metal for photocathodic protection.

The spray pyrolysis and hydrothermal techniques for ZnO on glass have been widely reported [18-20]. The structure of ZnO consists of clearly defined hexagonal nanorods, providing many areas for light absorption and electron generation. Fluorine-doped Tin Oxide glass (FTO) is a highly efficient substrate due to its electrically conductive surface, ease of synthesizing semiconductor materials, and versatility for various synthesis methods. FTO glass has garnered significant interest in research, as it can be used as a substrate for synthesizing various functional materials, including ZnO using the hydrothermal microwave method [21], $CuBi_2O_4$ template-assisted electrodeposition and oxidation reactions [22], or CIS/CdS/ZnO/ZnO:Al through electrodeposition [23], and many other syntheses techniques [24-27]. High electrical conductivity and ease of depositing various materials onto its surface make FTO glass a preferred substrate for diverse applications. There is no prior report on the application of heterostructure ZnS/ZnO nanorod films on a FTO glass, fabricated by the spray pyrolysis and hydrothermal techniques, as a photoanode for the photocathodic corrosion protection of a stainless steel under a 3.5 wt% NaCl solution.

In this study, we investigated the connectivity of ZnO and ZnS heterostructure nanorods synthesized on a FTO glass as photoanodes in the photoelectrochemical corrosion protection (PCP) for 304 stainless steel (SS304) in a 3.5 wt% NaCl solution. The fabrication process involved depositing ZnO onto a FTO glass with the hybrid spray pyrolysis and hydrothermal processes, followed by the hydrothermal deposition of ZnS onto the ZnO layer. The PCP performances of ZnO and ZnO/ZnS in a 3.5 wt% NaCl solution are analyzed and compared in this report.

2. Experimental methods

2.1 Preparation of ZnO/ZnS photoanodes

A ZnO film was synthesized on a 2.5 × 2.5 cm² FTO glass using a combination of spray pyrolysis and hydrothermal processes, the parametric details of the syntheses are reported [28] and [17]. The FTO glass was initially cleaned sequentially in the ultrasonic bath for approximately 15 min, using acetone, ethanol, and deionized water. To begin, the layer of ZnO seed was synthesized on the FTO glass through a spray pyrolysis. ZnO-seed precursors were sprayed for 1 h on the FTO glass, which was placed on a 400°C hot plate. The precursors consisted of 0.05 M of zinc acetate dihydrate ($(CH_3COO)_2Zn{\cdot}2H_2O$) dissolved in methanol. The growth of the ZnO layer on the seeded ZnO layer was achieved through a hydrothermal process at 90°C for 12 h, using a solution comprised of 0.025 M of zinc nitrate hexahydrate ($Zn(NO_3)_2{\cdot}6H_2O$) and 0.025 M of hexamethylenetetramine ($C_6H_{12}N_4$) in deionized water. Afterwards, the synthesized ZnO/FTO glass was dried at 100°C for 15 min. ZnS was subsequently synthesized by a hydrothermal process at 90°C for 7 h with 0.1 M thioacetamide solution. The heterostructure ZnO/ZnS film was then dried at 100°C for 15 min.

2.2 Characterizations of ZnO and ZnO/ZnS films

The crystal structures of the ZnO and ZnO/ZnS films were analyzed by X-ray diffractometer (Empyrean, PanAnalytical) equipped with a Cu Kα X-ray source (λ=1.540598 Å). The 2-theta range was scanned from 20° to 90°. An observation of the film surfaces was conducted using a scanning electron microscope (SEM) on a Hitachi microscope (SU3500) operated at 5 kV. The absorption of illumination was measured with UV-visible spectrophotometer (UV-1700 PharmaSpec, Shimadzu) in the range of wavelengths from 200 nm to 900 nm. The band gaps of ZnO and ZnO/ZnS were analyzed with Tauc plot technique.

2.3 Photoelectrochemical Analyses

A photoelectrochemical cathodic protection was measured using a PGSTAT100N under irradiation of UV-lamp (ULTRA-VITALUX). The PCP setup, as shown in Figure 1, consists of a corrosion cell and a photoelectrochemical cell. Both cells contained a 3.5 wt% NaCl electrolytes and were separated by a Nafion membrane for ion exchange. The corrosion cell comprised of a 304 SS working electrode, a Pt-coated mesh counter electrode and an Ag/AgCl reference electrode. The photoanode (ZnO or ZnO/ZnS), with an active area of 2.5 cm² × 2.5 cm², was placed in the photoelectrochemical cell. The photoanode was electrically connected with the 304 SS working electrode by a copper wire. The PCP analyses included the measurements of the open circuit potential (OCP), photocurrent, and polarization curve analysis (Tafel plot). A corrosion potential (E_{corr}) and a corrosion current density (j_{corr}) were obtained by polarization curves in the Tafel regions. Electrochemical impedance spectroscopy (EIS) of the ZnO and ZnO/ZnS photoanode films was conducted in a frequency range of 10^{-2} Hz to 10^{-5} Hz with an alternating current (AC) amplitude of 10 mV, both under illumination and dark conditions. The photocurrent was measured to investigate the photo-generated electrons from the photoanode to the SS304.

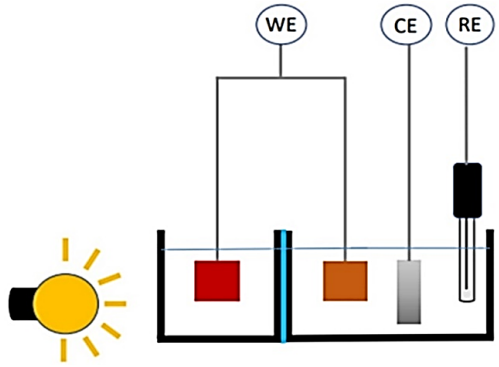


Figure 1. The diagram of the photocathodic protection (PCP) shows the WE as the working electrode, CE as the counter electrode and RE as reference electrode. The left cell is a photoelectrochemical cell containing a photoanode sample. The right cell is a corrosion cell containing a 304 SS sample, CE and RE.

3. Results and discussion

The X-ray diffraction (XRD) patterns of the ZnO and ZnO/ZnS films on FTO glass are presented in Figure 2. The characteristic 2θ peaks of the synthesized FTO glass are 26.61, 33.89 and 51.78 assigned to (110), (101) and (211) planes of SnO_2 from FTO glass substrates (JCPDS No. 41-1445). The peaks at 2θ = 31.85, 34.45, 36.35, 47.77, 56.65, 62.95, 68.00, and 69.12 align well with the (100), (002), (101), (102), (110), (103), (112), and (201) planes of hexagonal ZnO (JCPDS 36-1451) for the ZnO photoanode [8]. The ZnO and FTO corresponding peaks are present for the ZnO photoanode film, as shown in Figure 2(a). For ZnS, distinct peaks were detected at approximately 26.55 and 28.78, corresponding to the (102) and (001) diffraction peaks of ZnS (JCPDS 12-0688) [9]. The peak at 26.55° for ZnS overlapped with the peak at 26.61° for FTO. All the ZnS, ZnO, and FTO peaks are present for the ZnO/ZnS photoanode film (Figure 2(b)).

Figure 3 shows the morphology of the prepared samples. In Figure 3(a), the surface of ZnO nanorods appears fine structure with a hexagonal morphology. The diameter of the hexagonal ZnO nanorods is approximately 180 nm. In Figure 3(b), the cross-sectional picture reveals the ZnO seed layer with a thickness of approximately 460 nm, and ZnO nanorods grew on the seed ZnO with nanorod length of 1.64 µm. The ZnO seed layer aided in the growth of ZnO nanorod along the *c*-axis.

After growing ZnS on ZnO, the structure of ZnO/ZnS nanorods show no significant difference, as depicted in Figure 3(c). The ZnO/ZnS nanorods appeared larger than the ZnO nanorods both in size and length. The diameter of ZnO/ZnS nanorods is approximately 330 nm. Figure 3(d) shows a cross-section area of ZnO/ZnS nanorods. The ZnO/ZnS nanorods are taller than the ZnO nanorods with a length of 3.62 µm. The distributions of Zn, O, and S elements in ZnO/ZnS nanorods were analyzed using energy dispersive X-ray (EDX), as shown in Figure 4. All the elements are evenly distributed. The elemental fractions of the ZnO/ZnS nanorods are 22 wt% Zn, 51 wt% S, and 27 wt% O, as shown in Figure 5. The peaks of Zn, O and S indicate the deposition of ZnO/ZnS on FTO glass. Another peak is primarily Au, which is from a gold coating for SEM.

The light absorption was tested using ultraviolet-visible (UV-Vis) spectroscopy with slide glass as a reference. Figure 6(a) displays the absorbance of the ZnO and ZnO/ZnS films under UV lamp illumination, while Figure 6(b) shows the corresponding Tauc plots for determining the band energy gaps. The ZnO film exhibits an absorption edge at approximately 400 nm, indicating a band gap of about 3.2 eV. It strongly absorbs UV light, resulting in clear absorption and band gap characteristics. The absorption of the ZnO/ZnS film is broad ranging from 365 nm to 900 nm. The highest absorption spectrum of the ZnO/ZnS film occurred from 365 nm to 375 nm. This demonstrates its ability to absorb both visible light and UV light. The broad absorption range of the ZnO/ZnS is due to different band gaps of ZnO and ZnS. The band gap of the ZnO/ZnS film is measured to be 2.9 eV, as shown in Tauc plot of Figure 6(b). The heterostructure of ZnS/ZnO creates a new energy band gap due to the combination of ZnO and ZnS. The band structure is adjusted, leading to a lower energy band gap [29,30].

Figure 7(a) shows the open circuit potential (OCP) results of the 304 SS coupled with ZnO and ZnO/ZnS photoanodes under light on and off conditions. The OCP values stabilized, likely due to the equilibrium achieved between the generation and recombination of photogenerated electron-hole pairs [10]. For an uncoupled 304 SS, the OCP is within a narrow range of –0.1 V to 0.0 V vs. Ag/AgCl. Upon light illumination on the respective photoanodes, as shown in Figure 7(a), the 304 SS OCP negatively shifted to –0.27 V (by the ZnO/ZnS photoanode) and –0.2 V (by the ZnO photoanode) due to the supply of photogenerated electrons from the respective photoanodes. Upon turning off the light, the potential shifts back positively to that of base 304 SS. On the other hand, the recovery potential is slightly more negative than that of base 304 SS. Figure 7(b) represents the OCP values of the 304 SS coupled with the ZnO and ZnO/ZnS photoanode over an extended period: 2 h under illumination on the photoanodes and 5 h in the dark. It shows that the ZnO and ZnO/ZnS photoanode maintained its photocathodic protection for the 304 SS with the negatively-shift OCP throughout the illumination period. This capability provides long-term protection against pitting corrosion through photocathodic protection, if the light illumination on the photoanodes is available. Nevertheless, after the light was off, the OCP of the 304 SS increased back to the base value, but gradually decreased over time even under the dark condition. The final equilibrium OCP may be the combined OCP between the base 304 SS and the corresponding photoanodes under the dark condition.

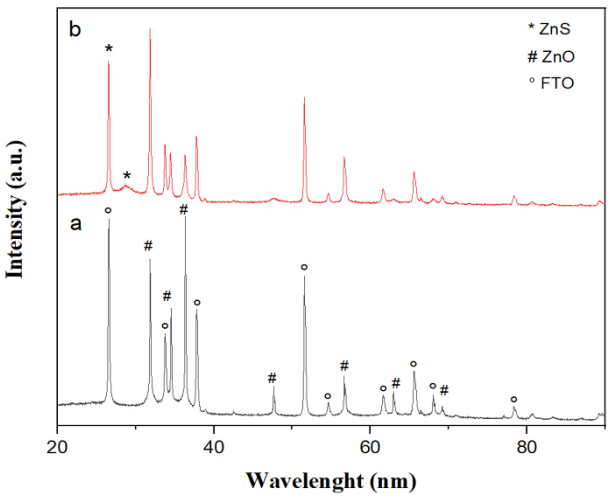


Figure 2. XRD patterns of the (a) is the ZnO, and (b) is the ZnO/ZnS photoanodes.

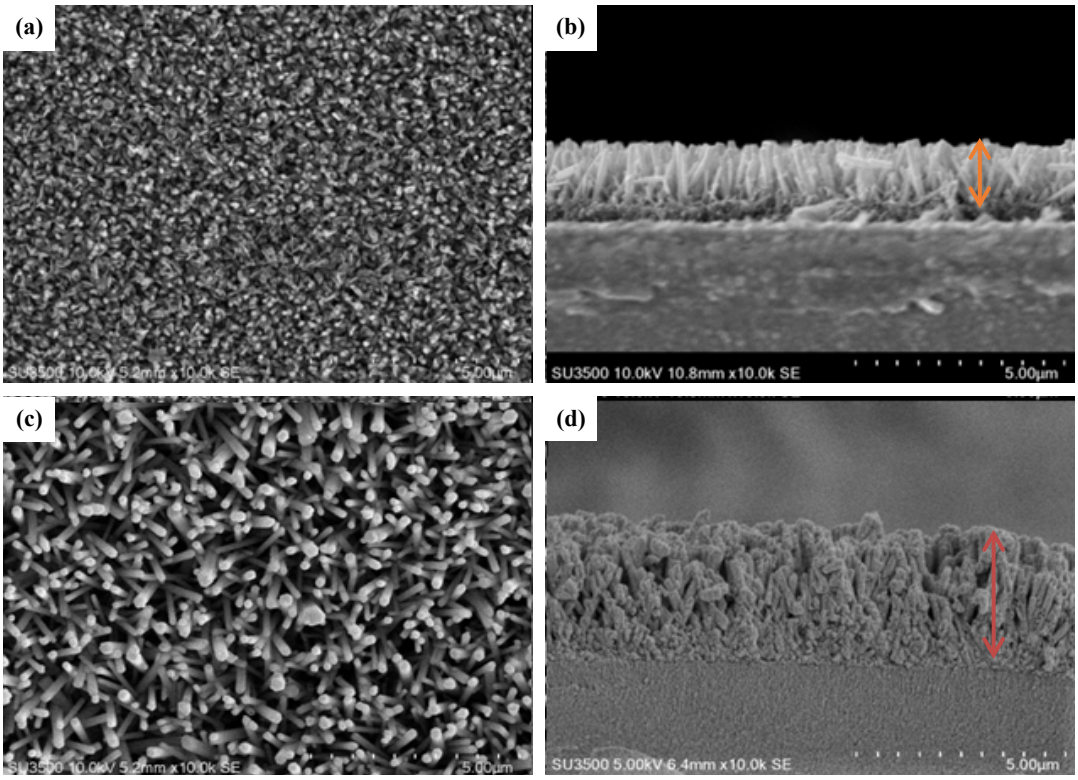


Figure 3. The morphological pictures of (a) ZnO (top view), (b) ZnO (cross-section), (c) ZnO/ZnS (top view), and (d) ZnO/ZnS (cross-section).

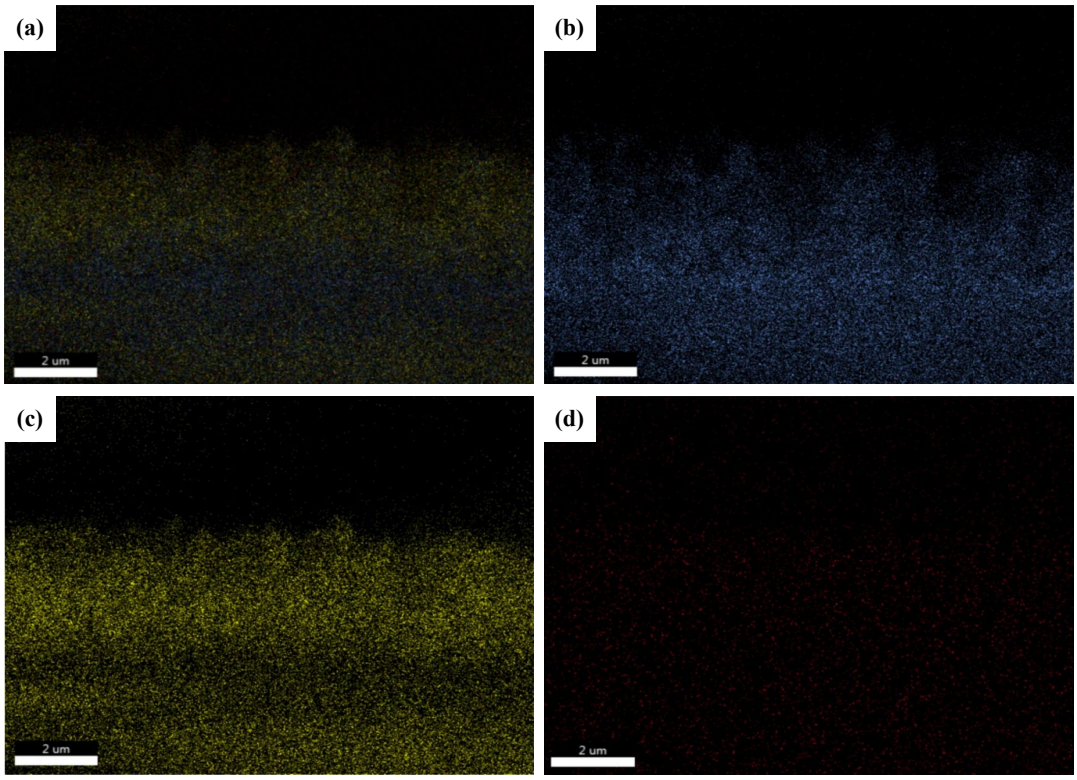


Figure 4. The distribution of elements in ZnO/ZnS nanorods using energy dispersive X-ray (EDX) analysis: (a) the elemental distribution for all elements, while (b), (c), and (d) show the distributions of oxygen, sulfur, and zinc, respectively.

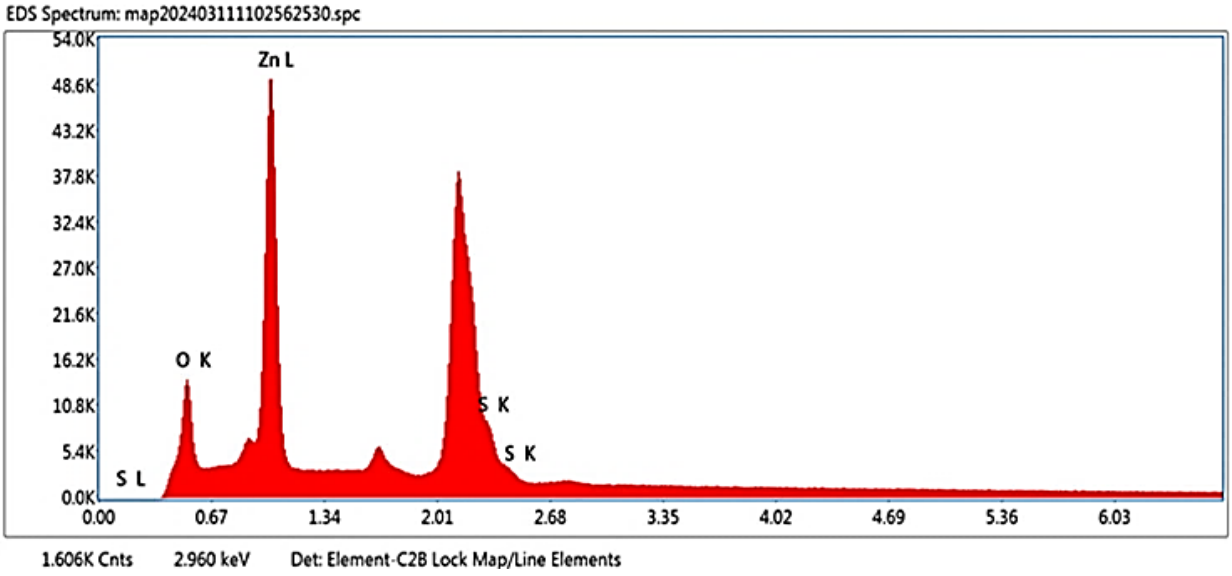


Figure 5. EDS spectrum and element analysis of the ZnO/ZnS nanorods on FTO glass.

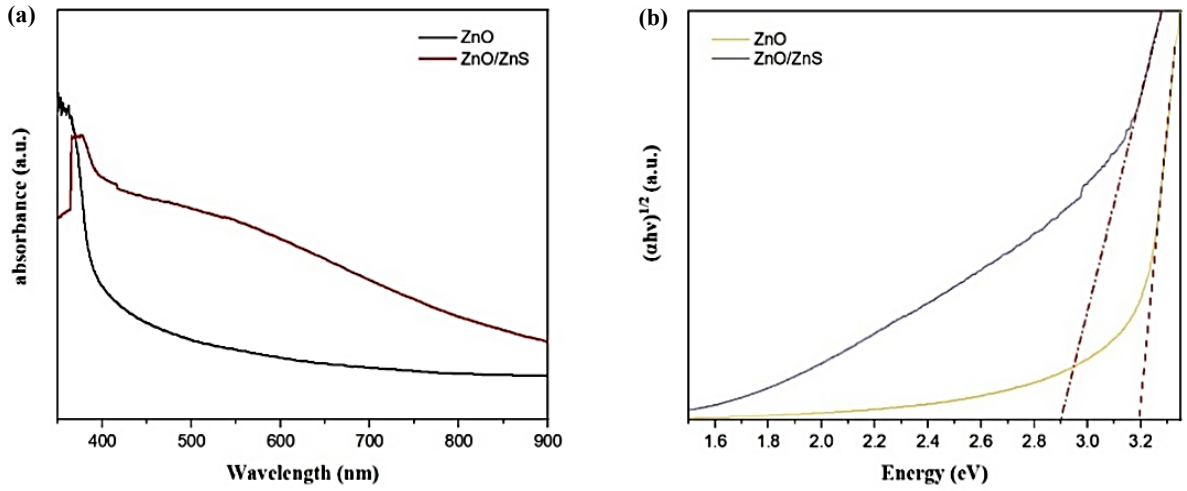


Figure 6. (a) Uv-Vis absorption spectra, and (b) the Tauc plot of ZnO/ZnS and ZnO photoanodes.

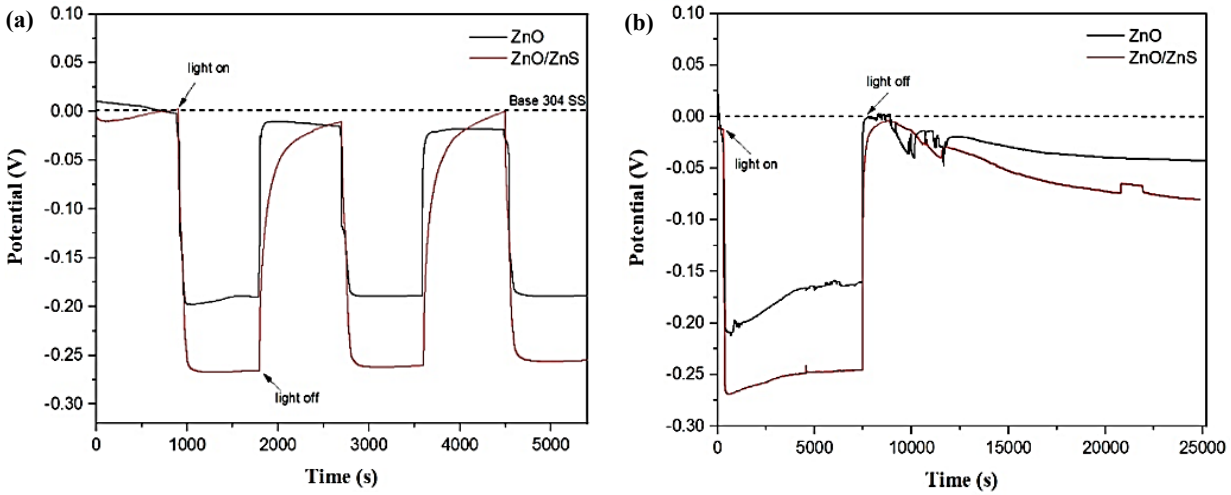


Figure 7. (a) Open circuit potential (OCP, vs. Ag/AgCl) of the 304 SS coupled with the ZnO, ZnO/ZnS photoanodes under light on and off cycles; (b) OCP test after light off for a long period.

Figure 8 shows the polarization curves of base 304 SS, 304 SS coupled with ZnO and ZnO/ZnS photoanodes. The corresponding corrosion potentials and current densities are summarized in Table 1. The corrosion potential (E_{corr}) of base 304 SS uncoated surface was –0.153 V vs. Ag/AgCl under the dark condition. When the 304 SS was coupled with ZnO and ZnO/ZnS photoanodes in the dark, the corrosion potentials were –0.152 V and –0.113 V, respectively. The E_{corr} of 304 SS coupled with ZnO is nearly the same as that of the base 304 SS. Although, the current intensity (j_{corr}) of 304 SS coupled with ZnO is higher than that of the base 304 SS (shown in Table 1). As a result, 304 SS coupled with ZnO loses electrons to the solution at a higher rate, respectively. Under illumination, the corrosion potentials for the 304 SS coupled with ZnO and ZnO/ZnS negatively shifted to –0.215 V and –0.289 V (vs. Ag/AgCl), respectively. The lower corrosion potential in the photocathodic protection suggests that photoanodes generated photo electron-hole pairs and transferred the electrons to protect the coupled metals. The ZnO/ZnS photoanode exhibited larger negative E_{corr} shift to 304 SS than did the ZnO photoanode. For the current density (summarized in Table 1), the ZnO/ZnS and ZnO photoanodes under light illumination slightly increased as compared to under the dark condition. Both current densities under light illuminations were higher than that of base 304 SS.

Figure 9 shows the photocurrent results of the ZnO and ZnO/ZnS photoanodes under light on and off conditions. At the onset of light on, the current increased sharply for both ZnO and ZnO/ZnS photoanodes. The photocurrent of the ZnO/ZnS photoanode (under light on) is higher than that of ZnO photoanodes. Therefore, ZnO/ZnS photoanode showed better photocathodic protection than ZnO photoanode with the supply of more photo-generated electrons to the coupled metal.

To analyze the charge transfer, electrochemical impedance spectra (EIS) measurements were conducted under the dark and illumination conditions. In Figure 10, all Nyquist plots can be fitted using the proposed Randles equivalent circuit (Figure 10(a)), comprising an electrolyte resistance (R_s), a charge transfer resistance (R_{ct}), and a constant phase element (CPE). In the dark condition, shown in Figure 10(b), the ZnO/ZnS photoanodes exhibit a higher charge transfer resistance (R_{ct}) compared to ZnO photoanodes. The R_{ct} values for ZnO/ZnS and ZnO photoanodes are 37227 Ω and 13948 Ω, respectively. This suggests that the electrical conductivity of ZnO photoanodes is higher than to that of ZnO/ZnS photoanodes. The R_s of ZnO and ZnO/ZnS photoanodes are 18 Ω and 7.14 Ω, respectively. Conversely, under illumination shown in Figure 10(a), the R_{ct} for both films decreased significantly. The R_{ct} for ZnO/ZnS became lower than that of ZnO, with R_{ct} values for ZnO/ZnS and ZnO photoanodes of 176.7 Ω and 323.3 Ω, respectively. This indicates that electron generation occurs under light for both ZnO/ZnS and ZnO, resulting in an increase in the electrical conductivity as compared to the dark condition. The lower R_{ct} under UV illumination for ZnO/ZnS film as compared to that of ZnO film agrees well with the OCP and Tafel plot analyses. The R_s values for ZnO/ZnS and ZnO photoanodes (under UV illumination) are approximately 8.27 Ω and 13.95 Ω, respectively, indicating lower charge transfer resistance between ZnO/ZnS photoanodes and the electrolyte. This suggests higher charge separation and transfer efficiency.

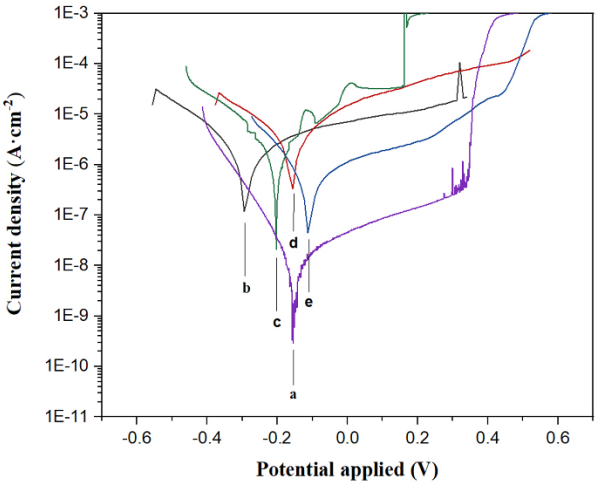


Figure 8. The polarization curves: (a) uncoated base 304 SS (dark condition), (b) and (e) are 304 SS coupled with ZnO/ZnS under illumination and dark conditions, respectively, (c) and (d) are 304 SS coupled with ZnO under illumination and dark conditions, respectively.

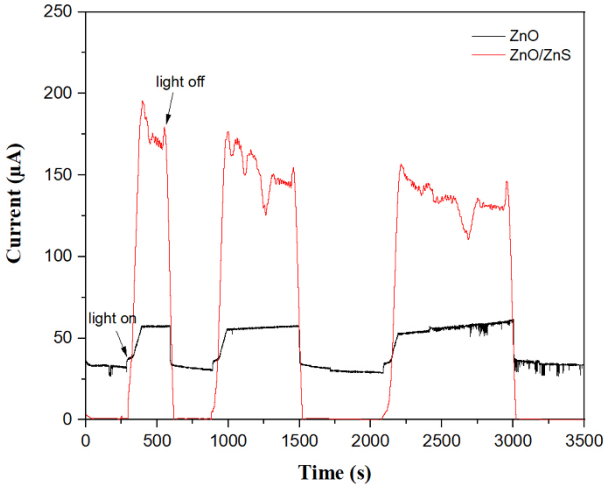


Figure 9. The photocurrent of the ZnO and ZnS/ZnS photoanodes under light on and off.

Table 1. The corrosion potentials (E_{corr}) and current densities (j_{corr}) of polarization of tafel plot for photocathodic protection.

Working electrodes	E_{corr} (V vs. Ag/AgCl)	j_{corr} [A·cm^{-2}]
304SS Base (uncoat and light off)	–0.153 ± 0.003	(1.16 ± 0.51) E-07
304SS-ZnO Light Off	–0.152 ± 0.003	(2.45 ± 1.59) E-06
304SS-ZnO Light On	–0.215 ± 0.021	(1.43 ± 0.254) E-06
304SS- ZnO/ZnS Light Off	–0.113 ± 0.003	(8.09 ± 1.07) E-06
304SS- ZnO/ZnS Light On	–0.289 ± 0.017	(5.02 ± 2.08) E-06

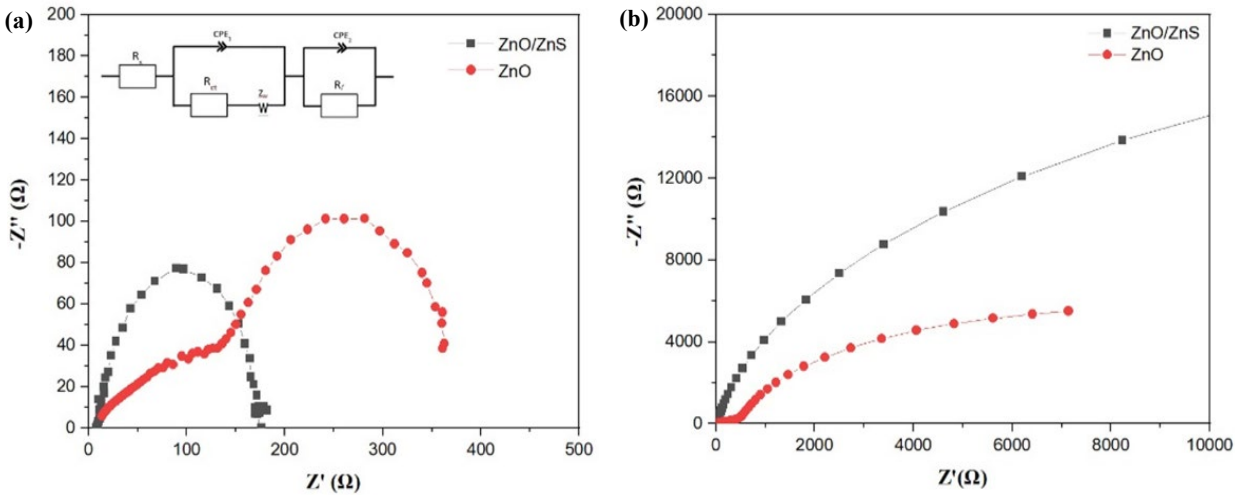


Figure 10. Nyquist plots of the ZnO and ZnO/ZnS photoanodes: (a) under UV illumination, and (b) in the dark.

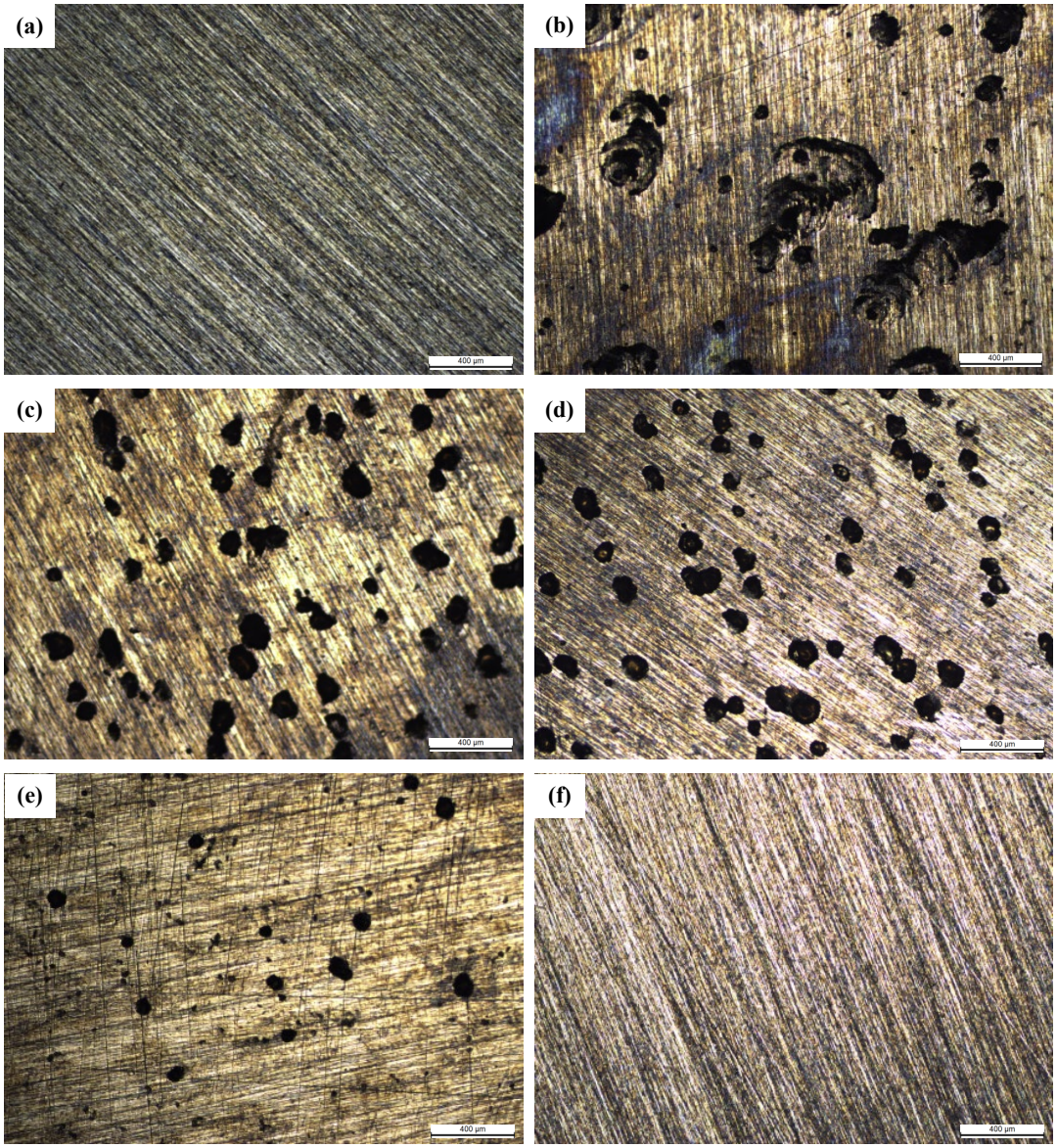


Figure 11. Optical microstructure (a) shows the surface of base 304 SS before polarization testing. Picture (b) – (f) show the OM structures of 304 SS samples after polarization testing with different conditions: (b) base 304 SS, (c) 304 SS coupled with ZnO under the dark condition, (d) 304 SS coupled with ZnO/ZnS under the dark condition, (e) 304 SS coupled with ZnO under UV illumination, and (f) 304 SS coupled withZnO/ZnS under illumination.

Figure 11 shows the optical microstructures of 304 SS before and after polarization testing, which support that the ZnO and ZnO/ZnS photoanodes could provide photocathodic protection under illumination. Figure 11(a) shows the base 304 SS before testing. After the polarization test in NaCl solution, as shown in Figure 11(b), the base 304 SS was significantly damaged by Cl^- ions with many large pitting holes. Under the dark condition, the 304 SS samples coupled with ZnO (Figure 11(c) and ZnO/ZnS (Figure 11(d)) showed corrosion of a few pitting holes, as there was no photocathodic protection in the absence of UV illumination. Under UV illumination, the 304 SS coupled with ZnO photoanode (shown in Figure 11(e)), showed fewer and smaller pitting holes as compared to the dark condition. For the 304 SS coupled with ZnO/ZnS photoanode (Figure 11(f)) showed clear photocathodic protection with no pitting corrosion observed even after polarization test. The results show both ZnO and ZnO/ZnS photoanodes could cathodically protect 304 SS in 3.5 wt% NaCl under UV illumination. And, the ZnO/ZnS photoanode showed better photocathodic performance than the ZnO one.

4. Conclusion

The ZnO and heterostructure ZnO/ZnS nanorod films were successfully synthesized on FTO substrates through the spray pyrolysis and a hydrothermal process. Tauc's plot analysis shows that the ZnO/ZnS film has lower bandgap than the ZnO film. The ZnO and ZnO/ZnS films were coupled with 304 SS to provide photocathodic protection under 3.5 wt% NaCl solution. The analyses of OCP, polarization curve and EIS indicated that the ZnO/ZnS photoanodes showed better photocathodic performance than the ZnO photoanodes with larger negative potential shifts and higher photo-generated current density under light illumination. The optical microstructures of the 304 SS samples after polarization testing evidently showed that, with UV illumination, the ZnO/ZnS photoanode effectively protected the 304 SS from pitting corrosion. In the absence of UV illumination, neither ZnO/ZnS heterostructure nor ZnO photoanodes showed photocathodic protection for the 304 SS. ZnO/ZnS heterostructure film is a promising candidate for photocathodic protection, as they are simple to fabricate with relatively low-cost materials. However, the addition of energy-storage materials should be considered to provide recurring protection in the absence of light.

References

[1] Dawei Xu, Yan Liu, Yunhao Zhang, Zeyao Shi, Mingkun Yang, Chen Zhang, and Bin Liu, "Fabrication of pyramid-$BiVO_4$/CdSe composite with controlled surface oxygen vacancies boosting efficient carriers' separation for photocathodic protection," *Chemical Engineering Journal*, vol. 393, p. 124693, 2020.

[2] Yuyu Bu, and Jin-Ping A, "A review on photoelectrochemical cathodic protection semiconductor thin films for metals," *Green Energy & Environment*, vol. 2, no. 4, pp. 331-362. 2017.

[3] A. H. Ettefagh, S. Guo and J. Raush, "Corrosion performance of additively manufactured stainless steel parts: A review," *Additive manufacturing,* vol 37, p. 101689, 2021.

[4] S. Chen, W. Chen, R. Yuan, H. Zhang, A. Elmarakbi, and Y.-Q. Fu, "Robust silica-graphene oxide nanocomposite membrane for separating NaCl salt from seawater under atmospheric pressure," *Desalination*, vol. 574, p. 117208, 2024.

[5] H. M. Lieth, R. Al-Sabur, R. J. Jassim, and A. Alsahlani, "Enhancement of corrosion resistance and mechanical properties of API 5L X60 steel by heat treatments in different environments," *Journal of Engineering Research*, vol. 9, no. 4B, 2021.

[6] H. M. Lieth, M. A. Jabbar, R. J. Jassim, and R. Al-Sabur "Optimize the corrosion behavior of AISI 204Cu stainless steel in different environments under previous cold working and welding," *Metallurgical Research & Technology,* vol. 120, no.4, 2023.

[7] Y. Lin, and S. Liu, "Robust ZnO nanowire photoanodes with oxygen vacancies for efficient photoelectrochemical cathodic protection," *Applied Surface Science,* vol. 566, 2021.

[8] Y. Bu, Z. Chen, J. Ao, J. Hou and M. Sun, "Study of the photo-electrochemical cathodic protection mechanism for steel based on the $SrTiO_3$-TiO_2 composite," *Journal of Alloys and Compounds*," vol. 731, pp.1214-1224, 2018.

[9] Y. Lin, and S. Liu, "Ion-exchange synthesis of ZnO/ZnSe/CdSe core/shell heterostructured nanowire photoanodes toward high-performance photocathodic protection of 304 stainless steel," *European Journal of Inorganic Chemistry,* vol. 2022, 2022.

[10] X. Zhang, G. Chen, W. Li, and D. Wu, "Preparation and photo-cathodic protection properties of ZnO/TiO_2 heterojunction film under simulated solar light," *Journal of Materials Science & Technology*, vol. 36, no. 8, pp. 1234-1240, 2020.

[11] V. S. Saji, "Review—photoelectrochemical cathodic protection in the dark: A review of nanocomposite and energy-storing photoanodes," *Journal of The Electrochemical Society*, vol. 167, no. 12, 2020.

[12] M. Yang, R. Jiang, J. Zhu, X. Zhang, G. Li, W.Li, F. Ma, X. Jiang, and H. Li, "Review on the solar-driven photocathodic protection of metals in the marine environment," *Coatings*, vol. 14, no. 3, p. 276, 2024.

[13] Y. Lin, and S. Liu, "Synthesis of ZnO/Bi_2S_3 core/shell nanowire array photoanodes for photocathodic protection of stainless steel," *Coatings*, vol. 12, no. 2, p. 244, 2022.

[14] H. Kim, M.-H. Oh, and B. L. Yang, "Photocorrosion of poly-aniline-ZnS-ZnO photoelectrode for water splitting," *Thin Solid Films*, vol. 693, p. 137678, 2020.

[15] N. Wei, Y. Lin, Z. Li, W. Sun, G. Zhang, M. Wang, and H. Cui, "One-dimensional Ag_2S/ZnS/ZnO nanorod array films for photocathodic protection for 304 stainless steel," *Journal of Materials Science & Technology*, vol. 42, pp. 156-162, 2020.

[16] R. Techapiesancharoenkij, W. Sripianem, K. Tongpul, C. Peamjharean, T. Na Wichean, T. Meesak, and P. Eiamchai, "Investigation of the photocathodic protection of a transparent ZnO coating on an AISI type 304 stainless steel in a 3% NaCl solution," *Surface and Coatings Technology*, vol.320, pp. 97-102, 2017.

[17] P. Wipataphan, J. Laohawattanajinda, T. Na Wichean, W. Sripianem, and R. Techapiesancharoenkij, "Photocathodic protection of amorphous and nanorod zinc oxide thin-film coatings on stainless steel AISI 304 fabricated by spray pyrolysis and hydrothermal technique," *Materials Chemistry and Physics*, vol. 291, p. 126714, 2020.

[18] A. A. Ryabko, A. I. Maximov, V. N. Verbitskii, V. S. Levitskii, V. A. Moshnikov, and E. I. Terukov "Two-stage synthesis of structured microsystems based on zinc-oxide nanorods by ultrasonic spray pyrolysis and the low-temperature hydrothermal method," *Technical Physics Letters*, vol. 46, no. 11, pp. 1071-1074, 2020.

[19] T. Tharsika, A. S. M. A. Haseeb, S. A. Akbar, and M. Thanihaichelvan, "Tailoring ZnO nanostructures by spray pyrolysis and thermal annealing," *Ceramics International*, vol. 41, no. 3, pp. 5205-5211, 2015.

[20] K. Mosalagae, D. M. Murape, and L. M. Lepodise, "Effects of growth conditions on properties of CBD synthesized ZnO nanorods grown on ultrasonic spray pyrolysis deposited ZnO seed layers," *Heliyon*, vol. 6, no. 7, 2020.

[21] P. Wipataphan, W. Sripianem, N. B. Oo, T. Na Wichean, B. Dachbumroong, O. Jongprateep, G. Panomsuwan, N. Pewnim, and R. Techapiesancharoenkij, "Photoelectrochemical cathodic protection of amorphous zinc oxide coating on hot rolled steel SS400 in a 3 wt% NaCl solution and a Na_2S-NaOH solution," *Journal of Metals, Materials and Minerals*, vol.31, pp. 129-142, 2021.

[22] G. de Souza, L. H. Nery, J. O. D. Malafatti, J. A. Dias, E. C. Paris, R. F. Klein-Gunnewiek, and T. Giraldi, "Zinc oxide films deposited on FTO substrate by hydrothermal microwave-assisted method," *MRS Communications*, vol. 12, pp. 409-414, 2022.

[23] Q. Zhang, B. Zhai, Z. Lin, X. Zhao, and P. Diao, "Dendritic $CuBi_2O_4$ array photocathode coated with conformal TiO_2 protection layer for efficient and stable photoelectrochemical hydrogen evolution reaction," *The Journal of Physical Chemistry C*, vol. 125, pp. 1890-1901, 2021.

[24] M. Esmaeili-Zare, and M. Behpour. "CIS/CdS/ZnO/ZnO: Al modified photocathode for enhanced photoelectrochemical behavior under visible irradiation: Effects of pH and concentration of electrolyte solution," *International Journal of Hydrogen Energy*, vol. 45, pp. 8273-8281, 2020.

[25] P. Qiu, Y. Lai, X. Sun, C. Chen, and L, Ge, "Potent n-type nanostructured cruciate flower-like Cu/Cu_2O films for photo-cathodic protection," *Materials Chemistry and Physics,* vol. 241, p. 122311, 2020.

[26] X. He, Y. Qu, S. Liao, J. Wang, J. Hu, and L Duan, "Preparation of multistage heterojunction composite film for round-the-clock photocathodic protection," *Surface and Coatings Technology,* vol. 465, p. 129593, 2023.

[27] J. Li, Y. Chu, C. Zhang, X. Zhang, C. Wu, X. Xiong, L. Zhou, and D. Han, "CoFe prussian blue decorated $BiVO_4$ as novel photoanode for continuous photocathodic protection of 304 stainless steel," *Journal of Alloys and Compounds*, vol. 887, p. 161279, 2021.

[28] W. Sripianem, and R. Techapiesancharoenkij, "Effect of Al and Ga cooping on the morphological, electronic, and optical properties of ZnO transparent conductive thin films prepared by spray pyrolysis technique," *Turkish Journal of Physics*, vol. 42, pp. 688-698, 2018.

[29] G. Hitkari, S. Singh, and G. Pandey, "Photoluminescence behavior and visible light photocatalytic activity of ZnO, ZnO/ZnS and ZnO/ZnS/α-Fe_2O_3 nanocomposites," *he Transactions of Nonferrous Metals Society of China*, vol. 28, no. 7, pp. 1386-1396, 2018.

[30] P. V. Raleaooa, A. Roodt, G. G. Mhlongo, D. E. Motaung, R. E. Kroon, and O, M. Ntwaeaborwa "Luminescent, magnetic and optical properties of ZnO-ZnS nanocomposites," *Physica B: Condensed Matter*, vol. 507, pp. 13-20, 2017.